Supplementary Materials for "On The Diffusion of Sticky Particles in 1-D"

Joshua DM Hellier* and Graeme J Ackland†
SUPA, School of Physics and Astronomy, University of Edinburgh, Mayfield Road, Edinburgh EH9 3JZ, United Kingdom
(Dated: June 5, 2018)

Lattice MFT Derivation. Let the ensemble-averaged occupation probability of the i^{th} site at time t be $\rho_i(t)$. In the mean-field approximation regime this is assumed to be independent of $\rho_j(t)$ for $j \neq i$ at equal times. Therefore we can condition upon the probability of the i^{th} site being occupied at a given time t simply by multiplying by $\rho_i(t)$. If the i^{th} site is full, then the rate at which it empties is the sum of the probabilities that the $(i+1)^{\text{th}}$ and $(i-1)^{\text{th}}$ sites are empty, multiplied by a rate which depends on the occupation probability of the $(i+2)^{\text{th}}$ and $(i-2)^{\text{th}}$ sites respectively. Therefore in the MFT the rate at which the i^{th} site empties is

$$\begin{aligned}&\frac{1}{\tau_0}(1-\rho_{i-1})\left[(1-\rho_{i+1})+\lambda\rho_{i+1}\right]\\ +&\frac{1}{\tau_0}(1-\rho_{i+1})\left[(1-\rho_{i-1})+\lambda\rho_{i-1}\right].\end{aligned} \tag{1}$$

Similarly, if the $(i)^{\text{th}}$ site is unoccupied, it fills with rate

$$\frac{1}{\tau_0}\left\{\rho_{i+1}\left[\lambda\rho_{i+2}+(1-\rho_{i+2})\right]+\rho_{i-1}\left[\lambda\rho_{i-2}+(1-\rho_{i-2})\right]\right\}. \tag{2}$$

If we now multiply the filling and emptying rates of site i by its occupation probability and the complement respectively, we obtain the final result that

$$\begin{aligned}\tau_0\frac{\partial\rho_i}{\partial t} =&(1-\rho_i)\left[(1-\zeta\rho_{i-2})\,\rho_{i-1}+(1-\zeta\rho_{i+2})\,\rho_{i+1}\right]\\ &-\rho_i\left[2\zeta\rho_{i-1}\rho_{i+1}-(3-\zeta)\left(\rho_{i-1}+\rho_{i+1}\right)+2\right].\end{aligned} \tag{3}$$

MFT Continuum Limit. To obtain the continuum limit of the MFT simply substitute $\rho_i(t) \to \rho(x,t)$, $\rho_{i+m}(t) \to \rho(x+am,t)$ into Eq. 3. Then, Taylor expand around x for small a, neglecting terms of $\mathcal{O}(a^4)$. Doing this and collecting terms we find that

$$\begin{aligned}\tau_0\frac{\partial\rho}{\partial t} =&a^2\left[1-\zeta\rho(4-3\rho)\frac{\partial^2\rho}{\partial x^2}\right]\\ &+2a^2\zeta(3\rho-2)\left(\frac{\partial\rho}{\partial x}\right)^2+\mathcal{O}(a^4),\end{aligned} \tag{4}$$

which can be factorized into the more familiar continuity equation

$$\frac{\partial\rho}{\partial t}=\frac{a^2}{\tau_0}\frac{\partial}{\partial x}\left\{\left[1-\zeta\rho\left(4-3\rho\right)\right]\frac{\partial\rho}{\partial x}\right\}, \tag{5}$$

having dropped the higher-order terms in the continuum limit.

Steady State Solution to the Continuum MFT. Eq. 5 is simple to solve in the time-independent steady state. Integrating both sides with respect to x and using the chain rule, we see that

$$J_0(x-x_0)=\int\mathrm{d}\rho\left[1-\zeta\rho\left(4-3\rho\right)\right]=\rho+\zeta(\rho-2)\rho^2. \tag{6}$$

J_0 and x_0 may be chosen to yield the desired boundary conditions, and the equation may then be inverted by solving a cubic to find $\rho(x)$.

Linear Stability of MFT Solution. Let $\rho_0(x)$ be a solution to the steady-state continuum MFT, and let us apply a small perturbation $\delta\rho(x,t)$. Let us also assume that ρ_0 is also slowly-varying in x, in the sense that $\delta\rho = o(\rho_0)$ and $\frac{\partial\rho_0}{\partial x} = o(\delta\rho)$, which should be approximately true for a large domain. Then substituting $\rho = \rho_0 + \delta\rho$ into the continuum-limit MFT and only the highest-order terms, we find that

$$\frac{\partial\delta\rho}{\partial t}=\frac{a^2}{\tau_0}\rho_0(4-3\zeta\rho_0)\frac{\partial^2\delta\rho}{\partial x^2}+o(\delta\rho). \tag{7}$$

Performing a Fourier transform (or rather, a suitable local equivalent) with respect to x to yield $\hat{\delta\rho}(k,t) = \delta\rho(x,t)$, this becomes

$$\frac{\partial\hat{\delta\rho}}{\partial t}=-k^2\frac{a^2}{\tau_0}\rho_0(4-3\zeta\rho_0)\hat{\delta\rho}. \tag{8}$$

This means that so long as $\zeta < \frac{3}{4}$, the RHS is always negative, and therefore small perturbations decay exponentially and all is well. However, if $\zeta > \frac{3}{4}$, there may be regions of the solution where $\rho_0(4-3\zeta\rho_0)$ becomes negative, causing small perturbations to grow exponentially with an emphasis on high-wavenumber (short-lengthscale) modes, which indicates linear instability.

Detailed Balance Proof. In Fig. 1 we see all the possible transitions which may occur between local configurations. Assume that the system is now on a ring, with L lattice sites and N particles. Let us label possible system configurations by ξ and let the number of adjacencies (or "bonds") between particles is $b(\xi)$. Now for our ansatz, assume that the probability of the system being in state ξ is $\lambda^{-b(\xi)}$. In the top and bottom diagrams of Fig. 1 we can see that the number of bonds on both sides is the same, as are the transition rates back and forth; thus our ansatz holds for these states, as it predicts the probabilities of the left and right configurations are the same.

FIG. 1.

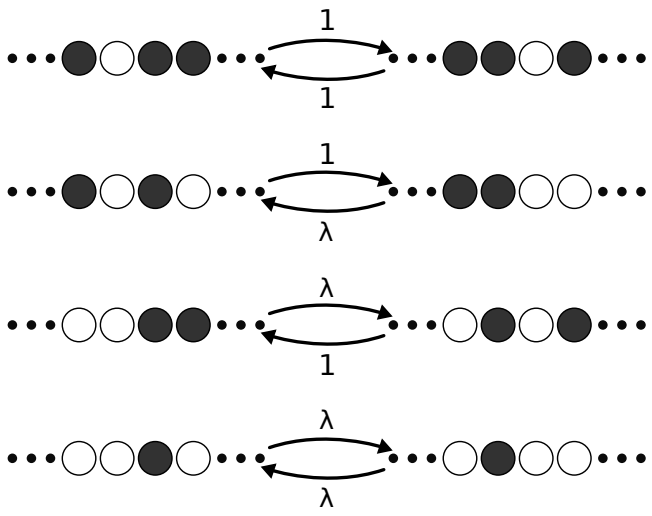

The middle two diagrams are the same only flipped; in the upper diagram a bond is formed going left to right and then broken going right to left, so the probability of being in the left state is λ times that of being in the right state. This is again in agreement with the detailed balance criterion. As these are the only types of transition that may occur on a ring, we may then say that the closed system obeys detailed balance.

Additional Flow Data. Fig. 2, 3 and 4 display additional data and information from computations discussed in the main body of the Letter.

More flow plots. For the interested reader we have included for spacetime flow diagrams, show in Fig. 5. When $\lambda = 0.05$, the medium consists of solid blocks surrounded by empty spaces containing a dilute gas of particles; at $\lambda = 0.35$ it is not so different from normal diffusion. The most interesting images are those for the intermediate λ; here we see a "lumpy" or "foamy" structure, in which small blocks of particles are being constantly created and destroyed whilst a rather minimal flow occurs across the system. The simulations did not show any hard phase transition as we vary λ; rather, it seems that this "foamy" behavior is part of a continuous range between the extremes, containing medium-range correlations between particles. Unfortunately, computing equal-time correlation functions to the accuracy required to draw conclusions about these correlations has proven to be extremely difficult, so we cannot find a quantitative description of the foam beyond the flow rate and density data we have discussed in this Letter. In all images in Fig. 5, long straight segments of white of black can be seen. The represent coherent motion at a characteristic velocity given by their gradient. There is nothing in the MFT to suggest what this velocity should be, and it is much smaller than the simulated system's length divided by the elapsed time, $\frac{L}{T}$, thus it must be an emergent property arising from correlated motion of self-assembled regions of high- or low-density material. However, it has again proved difficult to analyze this numerically.

Non-Uniqueness of the MFT Density Profile. Recall that, according to the MFT,

$$\int \mathrm{d}x\ J(x) = (x - x_0)J_0 = -\frac{a^2}{\tau_0}\rho\left[1 + \zeta\rho\left(\rho - 2\right)\right], \quad (9)$$

which we would like to solve for $\rho(x)$. We can do this uniquely so long as the right hand side is monotonic for $\rho \in (0, 1)$. Monotonicity requires that the sign of the derivative of the RHS wrt ρ does not change in that region. This derivative is of course

$$\frac{\mathrm{dRHS}}{\mathrm{d}\rho} = -\frac{a^2}{\tau_0}\rho\left[1 + \zeta\rho\left(\rho - 2\right)\right] = -\frac{a^2}{\tau_0}\left[3\zeta(\rho - \frac{2}{3})^2 + (1 - \frac{4}{3}\zeta)\right]. \quad (10)$$

The term in square brackets is always 1 at $\rho = 0$ and λ at $\rho = 1$, which are both positive. If $\zeta < 0$, the term is an n-shaped parabola with both boundaries positive; therefore it is always positive, and there is no sign change. For $\zeta > 0$ (the case of interest for us), we can see from completing the square that the term is always positive unless $\zeta > \frac{3}{4}$, in which case there is a sign change and therefore a loss of monotonicity. Thus for $\zeta > \frac{3}{4}$ (and correspondingly $\lambda < \frac{1}{4}$) the MFT does not have a unique steady state solution given a set of Dirichlet boundary conditions, and so we cannot expect the MFT to predict the density profile in that regime.

Particle Density in Bounded Domain at Extreme λ-Values. We scanned across a wide range of λ with three sets of boundary conditions: $(\frac{3}{10}, \frac{1}{10})$, $(\frac{3}{4}, \frac{1}{4})$ and $(\frac{9}{10}, \frac{7}{10})$. The resulting mean flow rate is show in Fig. 6, and mean density in Fig. 7. We once again see the transitions between power law behaviors, as discussed in the main body of the letter. Note that the MFT is never a particularly good fit for the $(\frac{3}{4}, \frac{1}{4})$ configuration; this may be because the difference between the boundaries is greater than in the other cases. The other MFTs are good fits in the high-λ regime until we start reaching $\lambda \sim 1000$, at which point they seem to start converging to the same flow regardless of boundary conditions. In each case for low-λ we have a power-law regime, each with with an exponent around 4, and then at extreme low-λ we lose a consistent signal because of noise, which we attribute to lack of system convergence due to critically slow flow.
So far as the density is concerned, at $\lambda = 1$ in each case it is about what we would expect (the average of the two boundary densities). It is minimized around $\lambda = 0.6$, and then as λ is reduced each density appears to converge to 1 regardless of boundary conditions (before we encounter the same convergence issue at extreme low-λ). As we go to high-λ, on the other hand, we see a similar convergence, but this time towards $\rho \sim 0.7$. This is interesting, as a density of $\rho = \frac{2}{3}$ is predicted by the MFT to be where maximal flow should occur for $\lambda > 1$; thus it

would appear that the system self-organizes to facilitate maximal flow, which is something which is hypothesized to occur in other nonequilibrium statmech systems. This also helps to explain the large deviations from the MFT flow predictions we encounter at high-λ, as the system in practice has a different density to the one assumed by the MFT.

* J.D.M.Hellier@sms.ed.ac.uk
† G.J.Ackland@ed.ac.uk

FIG. 2. Additional flow rate moments and overall system densities for the sweeps through λ with fixed boundaries.

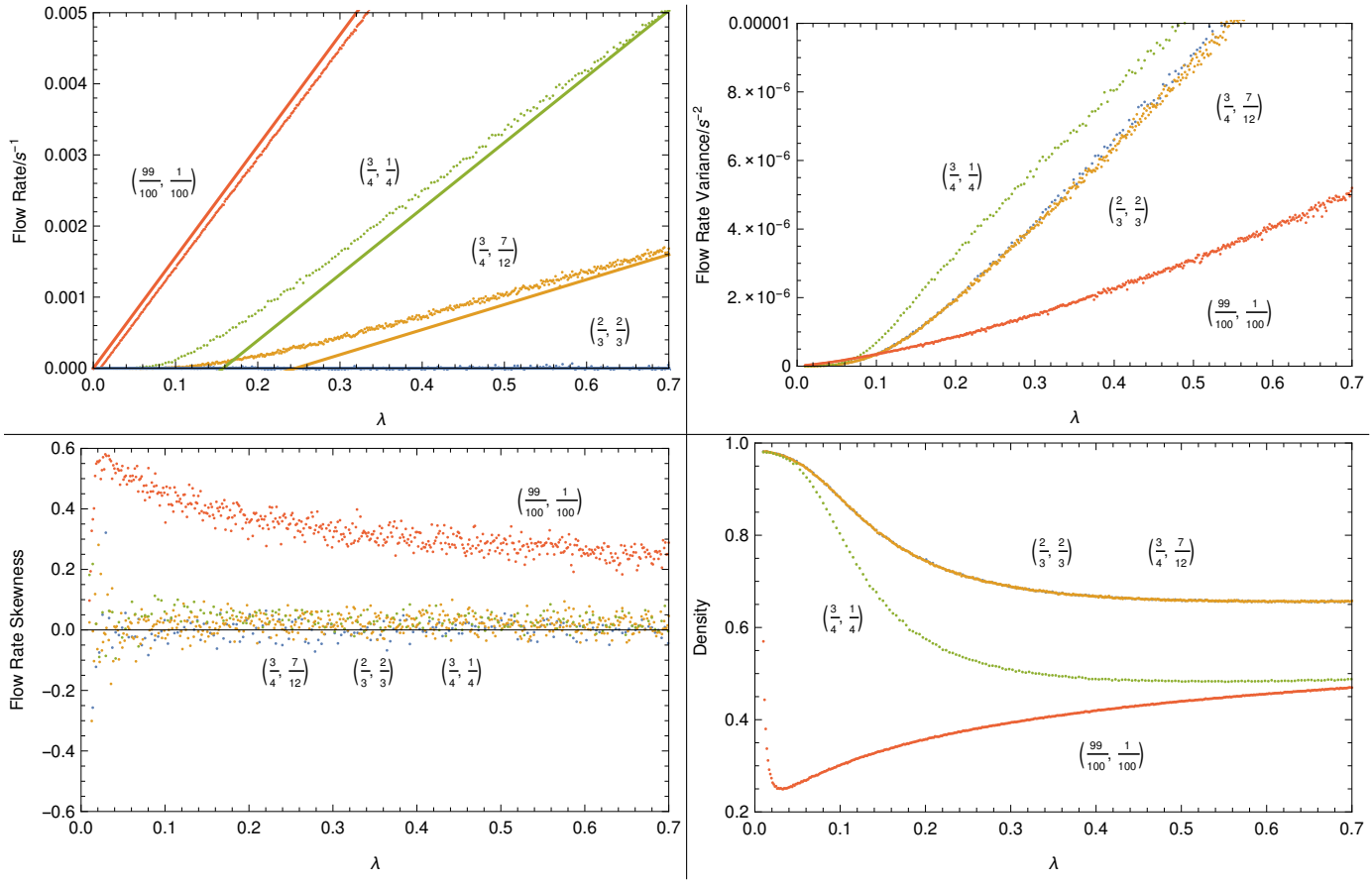

FIG. 3. Flow rate variance and average overall densities observed when varying the difference $\delta\rho$ between the boundary concentrations $(\rho_B, \rho_T) = (\rho_M + \frac{1}{2}\delta\rho, \rho_M - \frac{1}{2}\delta\rho)$ and λ. $\rho_M = \frac{1}{2}$, as in the Letter.

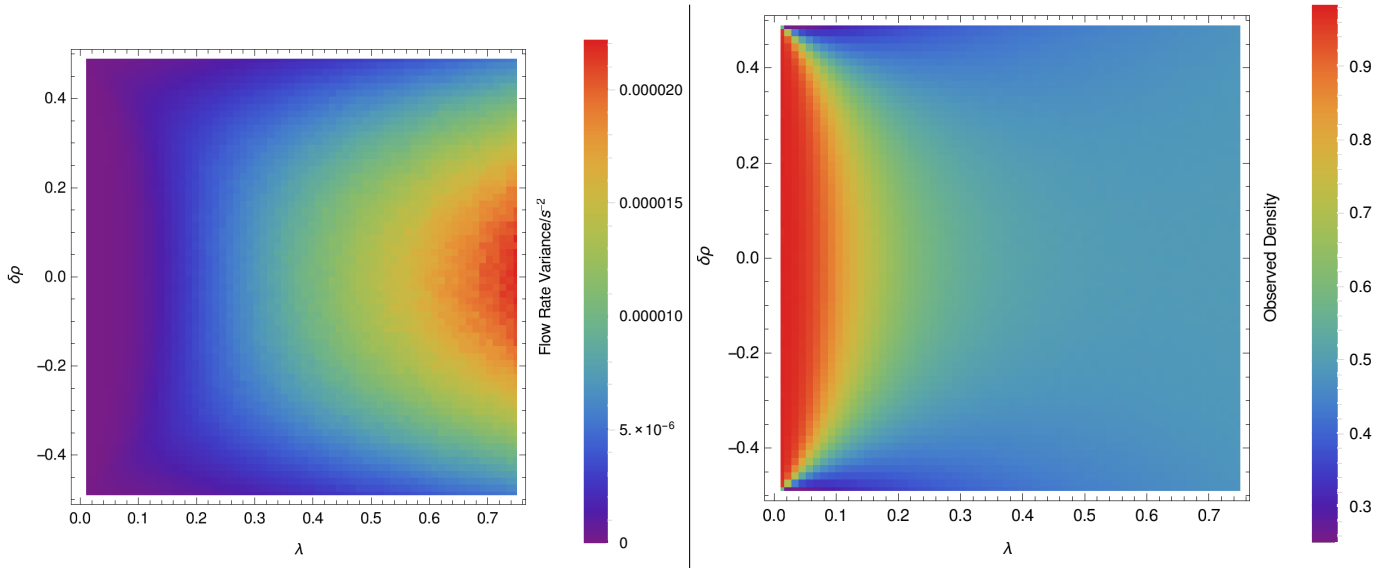

FIG. 4. These images are in addition to our computation of the effective diffusion coefficient D. The left shows the overall system density as a function of ρ_M and λ, whilst the right shows the standard error in our estimate of D. In this setup we ran the simulation for 1.6×10^8 equilibration steps, followed by 10 sets of alternating measurement and relaxation runs, of lengths 8×10^7 and 1.6×10^7 steps respectively. These results are consistent with calculations performed on smaller systems, so finite-size effects should be suppressed.

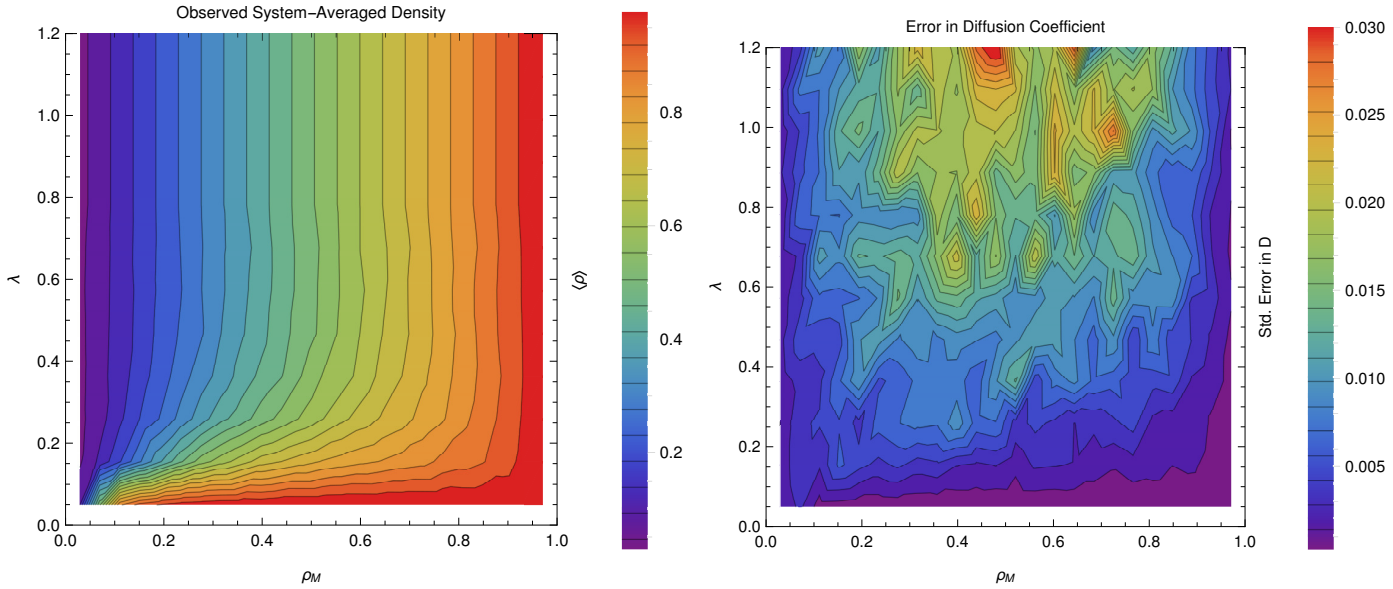

FIG. 5. The spacetime flow patterns, for λ-values of 0.05, 0.15, 0.25 and 0.35 going clockwise from top left. In each plot time runs along the x-axis, space along the y-axis, with the bottom boundary being held with a concentration of $\frac{1}{4}$ and the top at $\frac{3}{4}$. White represents full occupation, black empty, and gray shades partial occupation. The degree of occupation was calculated by taking the `KMCLib` record of a particular site's occupation (i.e. the Gillespie times at which the site changed occupation), assigning 0 and 1 to particles and vacancies respectively, linearly interpolating this and then integrating over times longer than a single Gillespie step but much shorter than the total time in question. In each case the total time elapsed is that taken by 2^6 Gillespie steps, and each short-time-average has been done over the total time divided by 512, the number of lattice sites; this means that on average a site would change state 8 times per pixel, although of course the real distribution is not nearly this even. Time has been rescaled this way in order to allow fair comparison of different λ-values.

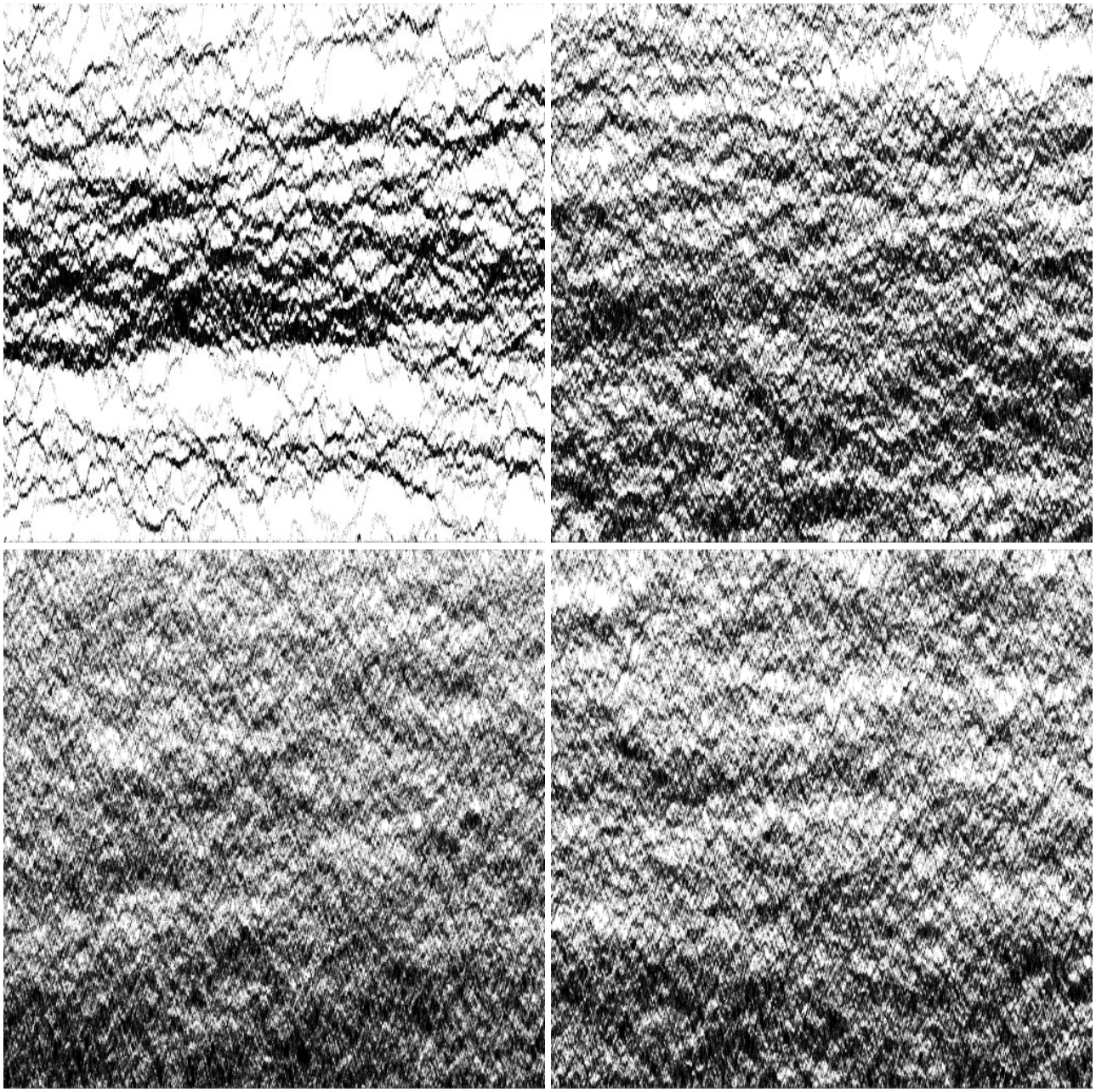

FIG. 6. Flow rate as a function of λ for systems with boundary conditions $(\frac{3}{10}, \frac{1}{10})$, $(\frac{3}{4}, \frac{1}{4})$ and $(\frac{9}{10}, \frac{7}{10})$, colored in blue, gold and green respectively.

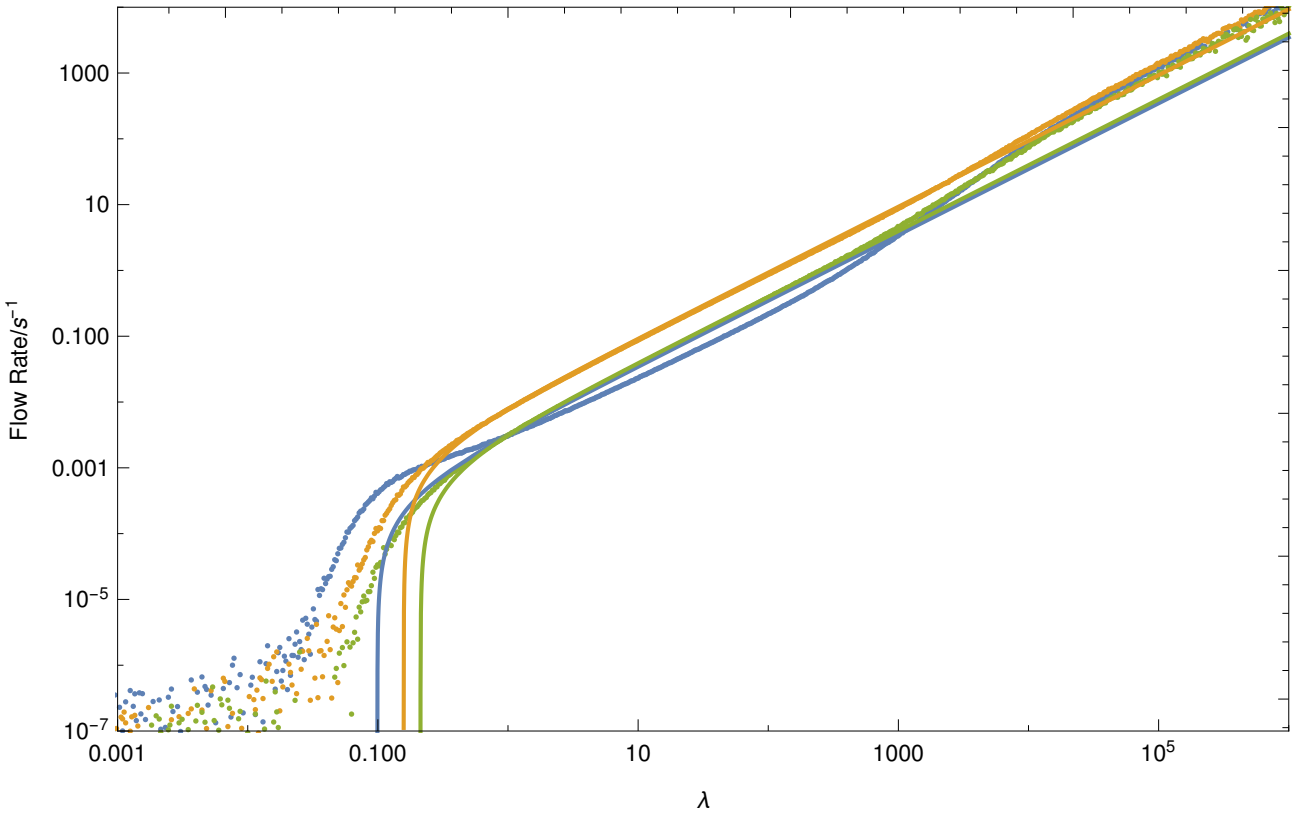

FIG. 7. Density as a function of λ for systems with boundary conditions $(\frac{3}{10}, \frac{1}{10})$, $(\frac{3}{4}, \frac{1}{4})$ and $(\frac{9}{10}, \frac{7}{10})$, colored in blue, gold and green respectively.